JCTC Journal of Chemical Theory and Computation

Quantum Electronic Structure

Time-dependent Complete Active Space Embedded in Polarizable Force Field

Hongbin Liu, Andrew J. Jenkins, Andrew Wildman, Michael J. Frisch, Filippo Lipparini, Benedetta Mennucci, and Xiaosong Li

J. Chem. Theory Comput., **Just Accepted Manuscript** • DOI: 10.1021/acs.jctc.8b01152 • Publication Date (Web): 28 Jan 2019

ACS Publications

is published by the American Chemical Society. 1155 Sixteenth Street N.W., Washington, DC 20036

Time-dependent Complete Active Space Embedded in Polarizable Force Field

Hongbin Liu,[†,‡] Andrew J. Jenkins,[†,‡] Andrew Wildman,[†] Michael J. Frisch,[¶] Filippo Lipparini,[§] Benedetta Mennucci,[§] and Xiaosong Li[*,†]

[†]*Department of Chemistry, University of Washington, Seattle, WA 98195*

[‡]*Authors contributed equally.*

[¶]*Gaussian Inc., 340 Quinnipiac St, Bldg 40, Wallingford, CT, USA 06492*

[§]*Dipartimento di Chimica e Chimica Industriale, Università di Pisa, Via Risorgimento 35, 56126 Pisa, Italy*

E-mail: xsli@uw.edu

Abstract

Electron correlation and environmental effects play important roles in electron dynamics and spectroscopic observables of chemical systems in condensed phase. In this paper, we present a time-dependent complete active space configuration interaction (TD-CASCI) approach embedded in a polarizable force field, MMPol. The present implementation of TD-CASCI/MMPol utilizes a direct matrix-vector contraction, allowing studies of large systems. This scheme is used to study the solvatochromic shift of coumarin 153 in methanol. The TD-CASCI/MMPol approach captures the double excitation character in the excited state wave function and accurately predicts the solvatochromic red-shift of coumarin 153 dye within the experimental range, outperforming linear response time-dependent density functional theory. The effect of using different reference orbitals for the TD-CASCI/MMPol simulation is also inves-

tigated, highlighting the need for an unbiased treatment of all electronic states in the energy-range of interest.

1 Introduction

Real-time time-dependent electronic structure theory seeks to solve the time-dependent Schrödinger equation (TDSE) for quantum systems in order to predict and simulate the response to external perturbations.[1–12] Real-time methods have been applied to many types of spectroscopy[13–16] as well as studies of charge migration and charge-transfer dynamics.[6,17–22] A commonly used real-time approach is the real-time time-dependent density functional theory (RT-TDDFT),[16,23–32] making use of TDDFT, one of the most prevalent methods for the study of excited state properties and absorption spectra of molecular systems. However, available DFT functionals used in RT-TDDFT are adiabatic, *i.e.* the exchange-correlation potentials do not change in time, and are designed for the ground state, leading to many known problems.[33–36]

Recently, wave function based real-time electronic structure theory in the framework of time-dependent configuration interaction (TD-CI) has been used for the calculation of absorption spectra and non-linear optical properties in vacuum.[37–41] Since the full TD-CI method is not computationally feasible except for very small molecular systems, the CI expansion is often truncated in terms of either the excitation operator (*e.g.*, singles and doubles) or the space used to construct the CI basis (*e.g.*, the complete active space approach). Both types of truncated TD-CI methods have shown promise in simulating multi-electron dynamics driven by external perturbations.[37,38,41]

An external perturbation of great chemical interest is the interaction between a molecule and its environment, such as a solvent or protein. It is well known that this perturbation can lead to changes in fundamentally dynamical properties of a molecule, as seen by solvatochromic shifts in spectra of chromophores[42–46] or solvent induced modifications to electron

transfer rates.[6] Although the importance of such a perturbation is widely recognized, care must still be taken when choosing a model to simulate the solute-solvent interaction. An effective and increasingly popular approach consists in adopting a so-called polarizable embedding scheme, which includes atomistic descriptions of the environment while also allowing for mutual polarization between the molecule and its environment. Many different models belong to the family of polarizable embedding, including, but not limited to the "Effective Fragment Potential Method"[47,48] and the polarizable molecular mechanics models, which can be based on induced dipoles[49–53] (MMPol), fluctuating charges,[54–57] or Drude oscillators.[58] Numerous recent efforts have been devoted to improving the accuracy of spectral simulations in an environment through the lens of polarizable embedding. Hedegård *et al.* implemented a multi-configuration self-consistent field (MCSCF) within their own polarizable embedding framework and used it to get the solvatochromic shift of the first absorption in acetone and uracil.[59] Li *et al.* combined the induced dipole formalism of MMPol with the complete active space self-consistent field (CASSCF)[60,61] method to accurately capture the solvation effect of water on the excited states of cytosine.[62] Donati *et al.* coupled real-time TDDFT to MMPol to simulate the absorption spectrum and the time-dependent dipole in both solvated systems as well as covalently bound protein.[63] Motivated by this final approach, this paper aims to merge the merits of both explicitly time-dependent complete active space (CAS) methods and MMPol to simulate the complex, environment-dependent and multi-electron excited state properties.

We present a time-dependent complete active space configuration interaction (TD-CASCI) method coupled with an MMPol environment. This method is then used to calculate the absorption spectrum of coumarin 153 (C153) in methanol, which has a pronounced and well studied solvatochromic shift, in order to highlight the need for both facets of the model. In addition, we explore the choice of reference orbitals for the TD-CASCI calculation and the implications of the choices on the behavior of the environment. In particular, the behaviors of TD-CASCI simulations using HF, ground state state-specific CASSCF (SS-CASSCF) and

state-averaged CASSCF (SA-CASSCF)[64] orbitals in an MMPol environment are compared to determine their suitability for capturing environmental effects on correlated excited states.

2 Theory

The time-evolving wave function of a many-electron system is governed by the time-dependent Schrödinger equation:

$$i\frac{\partial\Psi(t)}{\partial t} = \hat{H}(t)\Psi(t) \tag{1}$$

In the time-dependent configuration interaction (TDCI) framework, the wave function $\Psi(t)$ is expanded as a linear combination of time-independent Slater determinants $\{\Phi_i\}$:

$$\Psi(t) = \sum_k C_k(t)\Phi_k \tag{2}$$

where $\{C_i(t)\}$ are the time-dependent CI coefficients. Within a given basis, the TDCI approach gives the exact time-dependent variational solution of a many-electron system. However, it is not a computationally practical method except for small systems. For large molecules, the TDCI wave function expansion can be restricted in a so-called active space, resulting in a CAS formalism,

$$\Psi^{\mathrm{CAS}}(t) = \sum_{K\in\mathrm{CAS}} C_K(t)\Phi_K \tag{3}$$

As the size of the active space increases, the CAS wave function approaches the asymptotic limit of the full CI solution. In the following discussion, we remove the CAS denotation for simplicity, and use the following notation throughout the rest of the paper:

- $K, L, ...$ are Slater determinants in the *active* space.
- $t, u, v, w, ...$ are orbitals in the *active* space.
- $i, j, k, l, ...$ are orbitals in the *inactive* space.

- $a, b, c, d, ...$ are orbitals in the *virtual* space.
- $p, q, r, s, ...$ are any orbitals.
- $\nu, \nu', ...$ are atomic orbitals.

2.1 Time-dependent Complete Active Space Approach

With the CAS wave function ansatz in Eq. (3), Eq. (1) can be written in a matrix form as:

$$i\dot{\mathbf{C}}(t) = \hat{\mathbf{H}}(t)\mathbf{C}(t) \tag{4}$$

The Hamiltonian in the determinant basis is

$$\begin{aligned} H_{KL}(t) = \langle K| \sum_{tu} (h_{tu} + \sum_{i} (2(tu|ii) - (ti|iu)) + V_{tu}^{\mathrm{Ext}}(t))\, \hat{E}_{tu} \, |L\rangle \\ + \langle K| \frac{1}{2} \sum_{tuvw} (tu|vw)(\hat{E}_{tu}\hat{E}_{vw} - \delta_{uv}\hat{E}_{tw}) \, |L\rangle \end{aligned} \tag{5}$$

where the h_{pq} and $(pq|rs)$ are the one-electron and two-electron integrals, respectively. $\hat{E}_{pq}$ is an excitation operator

$$\hat{E}_{pq} = \hat{a}^{\dagger}_{p\alpha}\hat{a}_{q\alpha} + \hat{a}^{\dagger}_{p\beta}\hat{a}_{q\beta}. \tag{6}$$

The first term in Eq. (5) is the effective one-electron Hamiltonian which includes contributions from doubly occupied inactive orbitals and external perturbations. In the presence of an external electric field, $\boldsymbol{\xi}(t)$, the effect of the external perturbation takes on an electric-dipole approximation,

$$V_{tu}^{\mathrm{Ext}}(t) = \mathbf{d}_{tu} \cdot \boldsymbol{\xi}(t) \tag{7}$$

$$\mathbf{d}_{pq} = \langle p| \, \mathbf{r} \, |q\rangle \tag{8}$$

This potential is included in the effective one-electron Hamiltonian in Eq. (5)

2.2 Time-propagation of Direct TD-CASCI

Propagation of Eq. (4) can be carried out in the CI state basis where the time-evolution operator is a unitary matrix.[37,41,65] However, propagating the TD-CASCI wave function in the CI state basis requires a full diagonalization of the Hamiltonian and computation of the transition dipole matrix element between all CI states. This is not a computationally practical approach except for small CAS problems.

In this work, we use the second-order symplectic leapfrog method[38,66,67] to integrate the TD-CASCI equation in matrix form (Eq. (4)) with a *direct* algorithm to form the matrix-vector product.

The first step in the leapfrog propagation of Eq. (4) is a first order extrapolation of $\mathbf{C}$ at $t = 0$, $\mathbf{C}(0)$, to $\mathbf{C}$ at $t = \frac{\Delta t}{2}$, $\mathbf{C}(\frac{\Delta t}{2})$:

$$\mathbf{C}(\frac{\Delta t}{2}) = \mathbf{C}(0) + \frac{\Delta t}{2}\dot{\mathbf{C}}(0) \tag{9}$$

where $\dot{\mathbf{C}}(t)$ is written as the simple rearrangement of Eq. (4):

$$\dot{\mathbf{C}}(t) = -i\hat{\mathbf{H}}(t)\mathbf{C}(t) \tag{10}$$

The subsequent steps propagate $\mathbf{C}$ by evaluation of $\dot{\mathbf{C}}$ at the midpoint of the step:

$$\mathbf{C}(t) = \mathbf{C}(t - \Delta t) + \Delta t\ \dot{\mathbf{C}}(t - \frac{\Delta t}{2}) \tag{11}$$

The symplectic nature of the scheme ensures the norm is conserved over long-time propagation.[38]

The most time-consuming step of the leapfrog propagation is the evaluation of the matrix-

vector product in Eq. (10). In the *direct* TD-CASCI approach, the matrix-vector product

$$\sigma_L = \sum_L H_{KL} C_L \tag{12}$$

is computed *on-the-fly* using Olsen's minimum operation count algorithm.[68] Combining a *direct*-CI approach with the leapfrog algorithm results in a method with reduced memory requirements, allowing the use of larger CI expansions and the study of larger systems.

2.3 Coupling to the Time-dependent Polarizable Force Field

To describe the many-electron dynamics embedded in a polarizable force field, one needs to integrate the mutual polarization between the TD-CASCI and MMPol subsystems during the dynamics. MMPol introduces an additional time-dependent perturbation to the effective one-electron Hamiltonian,

$$V_{tu}^{\mathrm{MMPol}} = -\langle t| \sum_i \frac{q_i}{|\mathbf{r} - \mathcal{R}_i|} + \sum_p \frac{\boldsymbol{\mu}_p(t) \cdot (\mathcal{R}_p - \mathbf{r})}{|\mathbf{r} - \mathcal{R}_p|^3} |u\rangle \tag{13}$$

where $\{q_i\}$ are MM charges. Indices i and p label the charge and polarizable sites in the MM region, respectively. $\mathbf{r}$ are electronic degrees of freedom in the QM region and $\mathcal{R}$ are the nuclear degrees of freedom in the MM region.

The two terms in the bracket in Eq. (13) give rise to the electrostatic interaction between the QM electrons and the MM charges $\{q_i\}$ and induced dipole $\{\boldsymbol{\mu}_p\}$. The time-dependence of the MM dipoles $\{\boldsymbol{\mu}_p\}$ arises from the time-dependent electric field produced by the MM charges and QM electrons through the following linear equation,

$$\boldsymbol{\mu}_p(t) = \boldsymbol{\alpha}_p \cdot \left(\mathbf{E}_p(t) + \sum_{p' \neq p} S_{pp'}^{(3)} \frac{\boldsymbol{\mu}_{p'}(t)}{|\mathcal{R}_{pp'}|^3} - \sum_{p' \neq p} S_{pp'}^{(5)} \frac{3\mathcal{R}_{pp'}(\mathcal{R}_{pp'} \cdot \boldsymbol{\mu}_{p'}(t))}{|\mathcal{R}_{pp'}|^5} \right) \tag{14}$$

$$\mathbf{E}_p(t) = \sum_{i \neq p} q_i \frac{\mathcal{R}_p - \mathcal{R}_i}{|\mathcal{R}_p - \mathcal{R}_i|^3} + \sum_i Z_i \frac{\mathcal{R}_p - \mathbf{R}_i}{|\mathcal{R}_p - \mathbf{R}_i|^3} + \int \rho(\mathbf{r}, t) \frac{\mathcal{R}_p - \mathbf{r}}{|\mathcal{R}_p - \mathbf{r}|^3} d\mathbf{r} \tag{15}$$

where $\boldsymbol{\alpha}_p$ and $\mathbf{E}_p(t)$ are the static polarizability tensor and the time-dependent polarization field at the MM site p. $\mathbf{R}$ are nuclear degrees of freedom in the QM region. $S^{(3)_{pp'}}$ and $S^{(5)_{pp'}}$ are screening factors depending on the MM topology, which are introduced to avoid over-polarization effects.[69–71] In the MMPol scheme used in this work, atomic partial charges[72] and isotropic static atomic polarizabilities[50,73] in the MM region are employed.

The time-dependent polarization field at the MM site p includes the electric field produced by the time-dependent electronic density of charge $\rho(\mathbf{r}, t)$. In the current implementation, this term is evaluated as

$$\int \rho(\mathbf{r}, t) \frac{\mathcal{R}_p - \mathbf{r}}{|\mathcal{R}_p - \mathbf{r}|^3} d\mathbf{r} = \sum_{\nu\nu'} P_{\nu\nu'}(t) \langle \nu | \frac{\mathcal{R}_p - \mathbf{r}}{|\mathcal{R}_p - \mathbf{r}|^3} | \nu' \rangle \tag{16}$$

where $\mathbf{P}$ is the density matrix in the atomic orbital basis.

In this work, only the static polarizabilities of the MM sites are considered, and the MM induced dipoles respond instantaneously to the electric field produced by the time-dependent electronic density of charge $\rho(\mathbf{r}, t)$ at each polarizable site p. This is a reasonable and useful approximation for cases where the electric field generated by the QM region is oscillating much slower than the response in the MM region.[74]

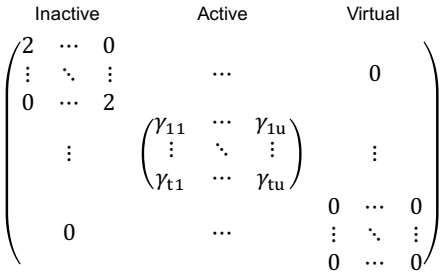

Figure 1. Density matrix $\boldsymbol{\gamma}$ in molecular orbital basis.

In the TD-CASCI formalism, the total one-particle density matrix takes on a form illustrated in Fig. 1 where all the inactive orbitals are doubly occupied and all virtual orbitals are empty. Only the one-particle density matrix in the active molecular orbital space depends

on times. Such a dependence stems from the time-evolution of TD-CASCI,

$$\begin{aligned}
&\gamma_{ii}(t) = 2, \quad \gamma_{ij}(t) = 0, \quad i \neq j \\
&\gamma_{tu}(t) = \langle 0| \hat{E}_{tu} |0\rangle = \sum_{KL} C_K^*(t) C_J(t) \langle K| \hat{E}_{tu} |L\rangle \\
&\gamma_{ab}(t) = 0
\end{aligned} \tag{17}$$

However, all electrons, including those in the inactive orbitals, produce polarization fields acting on the MM sites. Therefore, at each time step, the total one-particle density matrix in the molecular orbital space $\boldsymbol{\gamma}(t)$ is transformed to the atomic orbital space $\mathbf{P}(t)$ for the evaluation of the polarization field introduced by the QM region (Eq. (16)).

The computational cost of TD-CASCI is dominated by the matrix-vector product procedure, Eq. (12), which scales as $\mathcal{O}(N_{\text{det}}^2)$ where N_{det} is the number of determinants that grows factorially with respect to the CAS space. Compared to the TD-CASCI propagation in vacuum, there is an additional computational cost in the TD-CASCI/MMPol calculation due to the need to account for the mutual polarization of the QM and MM regions. This additional cost depends on the number of MM sites, N_{MM}, and the number of basis functions in the QM site, N_{QM}. As a result, the total computational cost of the TD-CASCI/MMPol method scales as $\mathcal{O}(N_{\text{det}}^2 + N_{\text{QM}}^2 N_{\text{MM}})$. For a simulation using a small CAS space and a large MM region, computing the MMPol polarization, Eq. (13), can become the computational bottleneck.

2.4 Computation of Absorption Spectrum and Signal Processing

In the *direct* TD-CASCI formalism, the time-dependent dipole moment can be computed as

$$\mu_{x,y,z}(t) = \text{Tr}[\mathbf{d}_{x,y,z} \boldsymbol{\gamma}(t)] \tag{18}$$

where $\mathbf{d}$ and $\gamma(t)$ are defined in Eq. (8) and Eq. (17). Note that only the time-evolving part of the one-particle density matrix can give rise to dipole oscillations and absorption signals.

The initial electric field perturbation corresponds to a step function lineshape lasting for only the initial time-step of width Δt, e.g.

$$\xi(t) = \begin{cases} \xi_{\max}, & 0 \leq t < \Delta t, \\ 0, & \text{else} \end{cases} \tag{19}$$

In this case, the discrete Fourier transform of the "delta pulse" $\xi(t)$ will simply be $\xi_{\max}$.

Following this external perturbation the molecular dipole will evolve in time. The absorption spectrum can then be determined by a Fourier transform of the time evolving dipole moment (Eq. (18)). Padé approximants, used in this paper, have been shown to produce comparable spectra with far shorter simulation time.[30,75] The transformed dipole moments can then be used to construct the isotropic dipole strength function

$$S(\omega) \propto \sum_{q=x,y,z} \mathrm{Tr}\left[\omega \cdot \mathrm{Im}\frac{\mu_q(\omega)}{\xi_q}\right] \tag{20}$$

to form the absorption spectrum.

3 Results and Discussion

3.1 Simulation Protocols

The TD-CASCI/MMPol method introduced in this work is implemented in the development version of the Gaussian software package.[76] The case study is the absorption spectrum of the coumarin 153 dye,[77–86] a member of a class of molecules widely employed as sensitizers in solar cells.[87] The time step used in the benchmark calculations is 0.024 attosecond to ensure an accurate interpretation of the results. TD-CASCI/MMPol dynamics are integrated for

15 fs. The external electric field employed to perturb the system had an intensity of 0.001 a.u., low enough to allow a linear approximation of the system response to the perturbation. Computed spectra are compared to experimental measurements and linear response TDDFT results. The PBE0 hybrid functional[88] with the 6-31G(d) basis set[89,90] is used in the TDDFT calculations. The same basis set is used for the TD-CASCI calculations.

3.2 Choosing the CASCI Space and Reference Orbitals

Characteristics of electron wave functions in TD-CASCI calculations strongly depend on the size of the active space and the choice of orbitals used to construct the configurations that expand the CAS wave function (Eq. (3)). Three different sets of molecular orbitals are used to construct the active space and their effects on the TD-CASCI spectra are investigated in this work. The three sets of molecular orbitals are fully optimized at the Hartree-Fock (HF) reference, ground state SS-CASSCF, and SA-CASSCF levels, respectively. In the following discussion, we will use TD-CASCI//HF, TD-CASCI//SS-CASSCF, and TD-CASCI//SA-CASSCF notations to describe the choice of molecular orbitals that underly the TD-CASCI simulations.

In order to determine the ideal size of the active space for TD-CASCI simulations, a large active space, CAS(22,16) (22 electrons and 16 orbitals), was initially investigated. We will use the optimized ground state HF reference orbitals in vacuum as a case study to illustrate the strategy to choose the active space. Ground state HF orbitals optimized in vacuum ranging from HOMO−10 to LUMO+4 are included in the CASCI(22,16) calculation. Suggested by a linear response TDHF calculation, these orbitals are mostly responsible for the lowest 15 electronic excitations. Fig. 2A shows orbital occupation numbers (Eq. (17)) obtained from the CASCI(22,16) calculation. Many orbitals are nearly doubly-occupied (occupation number > 1.95) or empty (occupation number < 0.05) in the lowest 16 CI states including the ground state. Only seven orbitals with significant π characters, HOMO−3 to LUMO+2 (see Fig. 2B), are considered active in terms of electron occupation number. This

analysis suggests that an active space of 8 electrons and 7 orbitals is sufficient for describing low-energy electronic excitations of coumarin 153 in vacuum. Similar exercises are used to select active spaces for TD-CASCI simulations using molecular orbitals optimized at different levels in vacuum and in MMPol (see Supporting Information, Figure S1 and S2), and result in the same size of active space for all simulations carried out in this work. Therefore, all following TD-CASCI calculations are performed in the CAS(8,7) framework with different optimized molecular orbital sets shown in Figure S2 in the Supporting Information. The initial condition at $t < 0$ before the field is turned on for each test case is chosen to be the ground state of the CASCI(8,7) solution.

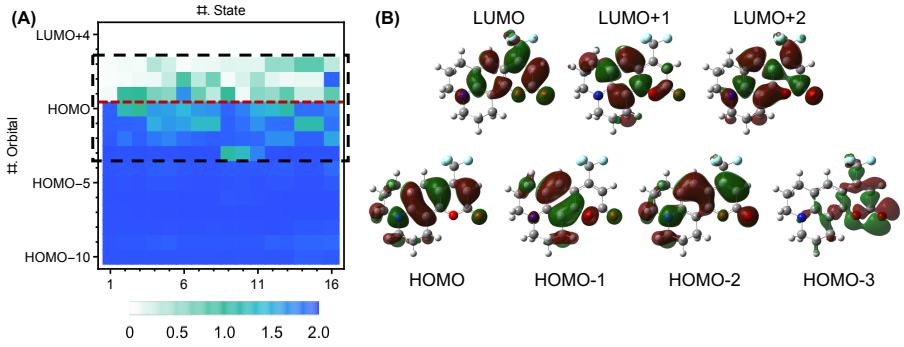

Figure 2. **(A)** Orbital occupation numbers, computed using Eq. (17), from HOMO−10 to LUMO+4 across the first sixteen states in coumarin 153. **(B)** Seven most *active* orbitals from the analysis in **(A)**.

Figure 3 shows absorption spectra of coumarin 153 in vacuum computed using three different TD-CASCI protocols, compared to those obtained with linear response TDDFT and TDHF. All TD-CASCI spectra are blue-shifted compared to those from linear response TDDFT and TDHF calculations. The spectral blue-shift in TD-CASCI is a result of a lack of dynamical correlation when a small active space is used. It should be noted that the TD-CASCI spectrum generated using SS-CASSCF ground state orbitals is more blue-shifted than those using HF and SA-CASSCF orbitals. This occurs because the SS-CASSCF orbitals are optimized solely for the ground state, meaning that the ground state is stabilized compared to the excited states. As a result, the energy gap between the ground and excited

states increases, causing a larger blue shift.

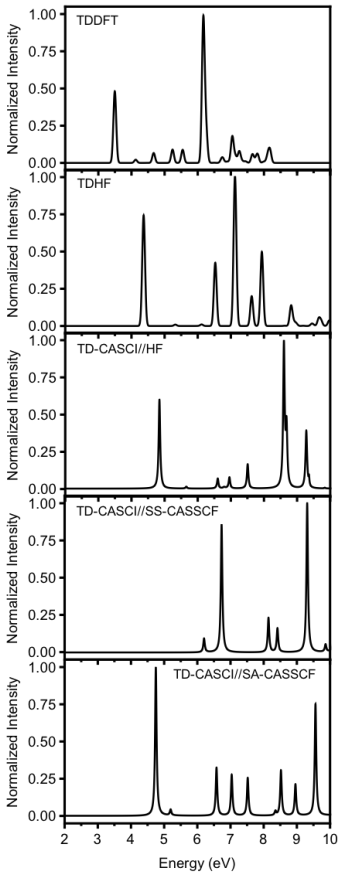

Figure 3. Absorption spectra of coumarin 153 in vacuum computed with linear response TDDFT, TDHF, and TD-CASCI using HF, SS-CASSCF, and SA-CASSCF optimized orbitals. Experimentally, the first absorption peak appears at 3.35 eV in vacuum.[85]

Figure 4 analyzes two characteristic absorption peaks in TDHF, TDDFT and TD-CASCI//HF spectra, including the first and the most intense peaks. Their contributing MO transitions and Slater determinants are shown with expansion coefficients. Compared to linear response TDDFT and TDHF calculations, most peaks in TD-CASCI//HF spectra consist of similar molecular orbital transitions that correspond to singly excited determinants. One major advantage of TD-CASCI over TDDFT or TDHF is that excited states containing characters beyond that of a single excitation can be resolved. Figure 4 shows that the two characteristic absorption peaks in TD-CASCI//HF spectrum contains double excitation contributions.

In particular, the first absorption peak of coumarin 153 in vacuum has a rather significant contribution from a doubly excited Slater determinant that corresponds to two-electron transition from HOMO to LUMO, a character that cannot be captured by linear response TDHF or TDDFT.

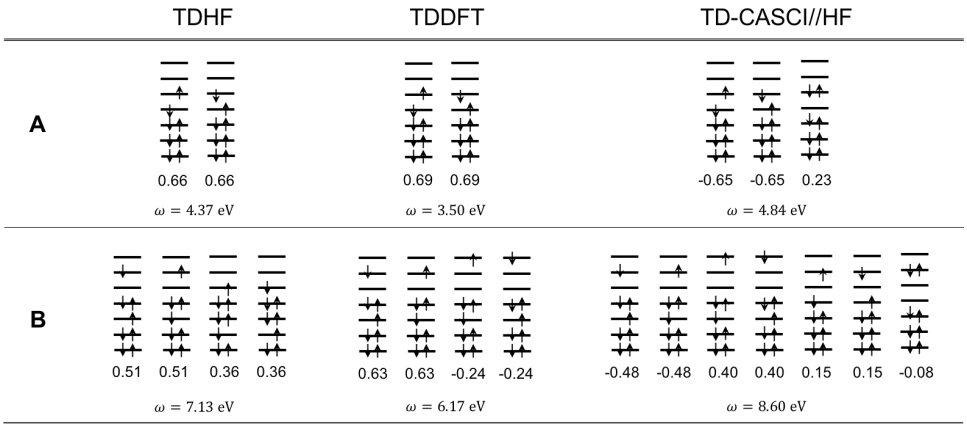

Figure 4. MO transition and Slater determinant contributions to the first, (**A**), and most intense, (**B**), absorption peaks for coumarin 153 in vacuum.

3.3 Solvatochromic Spectral Shift

The focus of this work is to illustrate the time-dependent interplay between solute electronic excited states and a polarizable environment, and how their interactions manifest in a solvatochromic shift. Therefore, although the absolute absorption peak positions are blue-shifted, we expect that the relative solvatochromic shifts can still be accurately captured by TD-CASCI since they arise due to the perturbation from the environment instead of internal electron correlation.

Experimentally, the lowest absorption peak of coumarin 153 in methanol exhibits a 0.35∼0.44 eV solvatochromic red-shift compared to that in vacuum.[85,91,92] The TD-CASCI/MMPol electronic dynamics of the coumarin 153 dye in methanol solvent are simulated to resolve the absorption spectrum and solvatochromic shift. Coumarin 153 was placed in a box of 175 methanol molecules.[93,94] The solvation box was previously equilibrated using the Amber parm99SB force field.[95–97]

To simulate electronic dynamics driven by external electric field in solvent, the system is initially prepared in equilibrium with the environment. In other words, molecular orbitals are variationally optimized in the presence of solvent before the external perturbation is turned on. The three self-consistent approaches, including HF, SS-CASSCF, and SA-CASSCF, to obtain molecular orbitals for the active space also represent three different equilibrium conditions to include the solvent effect at $t < 0$. Although at $t > 0$, the time-dependent interaction between the TD-CASCI quantum system and the MMPol subsystem is modeled in the same framework as described in Sec. 2.3 for all test cases, the electronic dynamics and spectroscopic signals strongly depend on the initial equilibrium conditions.

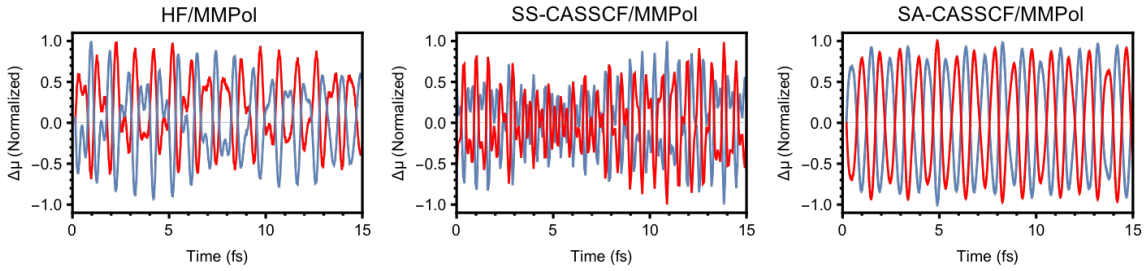

Figure 5. Normalized time-dependent net dipole moments of coumarin 153 in methanol after a delta-pulse perturbation, simulated with TD-CASCI/MMPol using different sets of orbitals. The net dipole moments of the QM region are plotted in blue, the net dipole moments of the MM region are plotted in red and have been magnified for 10 times. *left to right*: orbitals optimized at the HF/MMPol, SS-CASSCF/MMPol, and SA-CASSCF/MMPol levels.

Figure 5 shows the normalized time-dependent net dipole moments of coumarin 153 in methanol simulated with TD-CASCI/MMPol using solvated orbitals optimized at the HF/MMPol, SS-CASSCF/MMPol, and SA-CASSCF/MMPol levels. Time-dependent net dipole moments of the MMPol region are also plotted. Since the MM dipoles are propagated instantaneously with the perturbed QM electronic density, an anti-oscillatory behavior of the time-dependent MM dipole is expected. The absorption spectra obtained from the three dipole time series are compared in Fig. 6 to the results in vacuum and those obtained with linear response TDDFT/MMPol and TDHF/MMPol calculations in methanol.

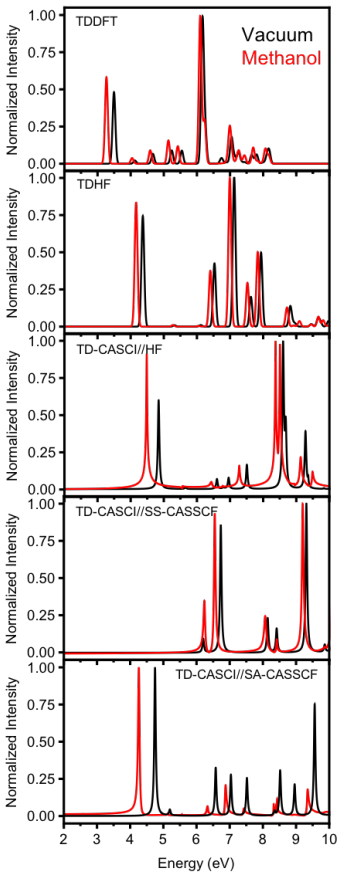

Figure 6. Absorption spectra of coumarin in methanol computed with TD-CASCI/MMPol using HF/MMPol, SS-CASSCF/MMPol, and SA-CASSCF/MMPol optimized orbitals (red) compared to their corresponding vacuum spectra (black).

Linear response TDHF and TDDFT exhibit a solvatochromic red-shift of 0.20 eV and 0.24 eV, respectively. In contrast, TD-CASCI simulations using the HF or SA-CASSCF optimized orbitals show a solvatochromic red-shift of of 0.37 eV and 0.44 eV, respectively, for the first absorption peak, in excellent agreement with experimental measurements. From the analysis in Fig. 4, this is attributed to the inclusion of higher order excitation contributions which are beyond the capability of linear response TDHF or TDDFT formalisms. However, the simulations using SS-CASSCF orbitals shows the smallest solvatochromic shift. This again is due to the fact that solvated orbitals are solely optimized for the ground state. In the cases of TD-CASCI using solvated HF and SA-CASSCF orbitals, both ground and

excited states are treated on an equal footing with the consideration of static correlation and environmental effects. This is an intrinsic nature of the TD-CASCI//HF approach. For TD-CASCI//SA-CASSCF, all relevant states should be considered in the state-average optimization of the solvated orbitals. In the case studied here, the lowest eight states are included in the averaging.

4 Conclusion

In this article, we have introduced a coupling scheme that embeds the TD-CASCI method in a polarizable force field, MMPol. The time-evolution of TD-CASCI approach employs a direct matrix-vector contraction *on-the-fly* which allows studies of large scale systems using the TD-CI approach.

The solvatochromic shift of coumarin 153 dye in methanol was studied using the TD-CASCI/MMPol approach developed in this work, compared to experimental measurements and results from linear response TDHF and TDDFT calculations. Although absolute excitation energies from TD-CASCI/MMPol simulations are higher than those calculated using TDHF and TDDFT due to the lack of dynamic correlation, TD-CASCI simulations using HF and SA-CASSCF solvated orbitals out-perform linear response TDHF and TDDFT for the computed solvatochromic shift. The TD-CASCI approach is particularly advantageous because its multi-configurational nature allows the description of the excited states with double-excitation character.

The effect of using different reference orbitals for the TD-CASCI simulation has also been investigated. The use of SS-CASSCF/MMPol solvated orbitals is discouraged because they give rise to a strong bias toward electronic characteristics of the ground state. In order to properly describe the excited state solvatochromic shift, wave functions of all relevant states should be treated on an equal footing. This is the case in the TD-CASCI simulations using HF and SA-CASSCF solvated orbitals which produce a solvatochromic red-shift in excellent

agreement with experiments.

The TD-CASCI/MMPol method detailed here is a powerful tool for studying electronic dynamics embedded in a polarizable environment. This method is particularly advantageous when excited states of the quantum subsystem are multi-configurational in nature.

Acknowledgement

The development of the solvated electronic dynamics is funded by the US Department of Energy (DE-SC0006863 to XL). AW is partially supported by IDREAM (Interfacial Dynamics in Radioactive Environments and Materials), an Energy Frontier Research Center funded by the U.S. Department of Energy (DOE), Office of Science, Basic Energy Sciences (BES). The development of *ab initio* linear response theory is supported by the US National Science Foundation (CHE-1565520 to XL). FL and BM gratefully acknowledge funds from the PRA_2018_36 project. AW is grateful for the support from the NSF Research Traineeship Program (DGE-1633216). Computations were facilitated through the use of advanced computational, storage, and networking infrastructure provided by the Hyak supercomputer system at the University of Washington, funded by the Student Technology Fee, and the National Science Foundation (MRI-1624430).

Supporting Information Available

Active space orbitals and Cartesian coordinates of coumarin 153 can be found in the supporting information.

References

(1) Ullrich, C. A.; Reinhard, P. G.; Suraud, E. Electron Dynamics in Strongly Excited Sodium Clusters: A Density-Functional Study with Self-Interaction Correction. *J. Phys. B* **1998**, *31*, 1871–1885.

(2) Lein, M.; Kreibich, T.; Gross, E. K. U.; Engel, V. Strong-Field Ionization Dynamics of a Model H2 Molecule. *Phys. Rev. A* **2002**, *65*, 033403.

(3) Schlegel, H. B.; Smith, S. M.; Li, X. Electronic Optical Response of Molecules in Intense Fields: Comparison of TD-HF, TD-CIS, and TD-CIS(D) Approaches. *J. Chem. Phys.* **2007**, *126*, 244110.

(4) Baer, R.; Gould, R. A Method for ab initio Nonlinear Electron-density Evolution. *J. Chem. Phys.* **2001**, *114*, 3385–3392.

(5) Liang, W.; Chapman, C. T.; Ding, F.; Li, X. Modeling Ultrafast Solvated Electronic Dynamics Using Time-Dependent Density Functional Theory and Polarizable Continuum Model. *J. Phys. Chem. A* **2012**, *116*, 1884–1890.

(6) Chapman, C. T.; Liang, W.; Li, X. Solvent Effects on Intramolecular Charge Transfer Dynamics in a Fullerene Derivative. *J. Phys. Chem. A* **2013**, *117*, 2687–2691.

(7) Ding, F.; Lingerfelt, D. B.; Mennucci, B.; Li, X. Time-Dependent Non-Equilibrium Dielectric Response in QM/Continuum Approaches. *J. Chem. Phys.* **2015**, *142*, 034120.

(8) Chapman, C. T.; Liang, W.; Li, X. Open-System Electronic Dynamics and Thermalized Electronic Structure. *J. Chem. Phys.* **2011**, *134*, 024118.

(9) Nguyen, T. S.; Nanguneri, R.; Parkhill, J. How Electronic Dynamics with Pauli Exclusion Produces Fermi-Dirac Statistics. *J. Chem. Phys.* **2015**, *142*, 134113.

(10) Nguyen, T. S.; Parkhill, J. Nonadiabatic Dynamics for Electrons at Second-Order: Real-Time TDDFT and OSCF2. *J. Chem. Theory Comput.* **2015**, *11*, 2918–2924.

(11) Nguyen, T. S.; Parkhill, J. Nonradiative Relaxation in Real-Time Electronic Dynamics OSCF2: Organolead Triiodide Perovskite. *J. Phys. Chem. A* **2016**, *120*, 6880–6887.

(12) Goings, J. J.; Lestrange, P. J.; Li, X. Real-Time Time-Dependent Electronic Structure Theory. *WIREs Comput. Mol. Sci.* **2018**, *8*, e1341.

(13) Lee, K. M.; Yabana, K.; Bertsch, G. F. Magnetic Circular Dichroism in Real-Time Time-Dependent Density Functional Theory. *J. Chem. Phys.* **2011**, *134*, 144106.

(14) Ding, F.; Van Kuiken, B. E.; Eichinger, B. E.; Li, X. An Efficient Method for Calculating Dynamical Hyperpolarizabilities Using Real-Time Time-Dependent Density Functional Theory. *J. Chem. Phys.* **2013**, *138*, 064104.

(15) De Giovannini, U.; Brunetto, G.; Castro, A.; Walkenhorst, J.; Rubio, A. Simulating Pump–Probe Photoelectron and Absorption Spectroscopy on the Attosecond Timescale with Time-Dependent Density Functional Theory. *ChemPhysChem* **2013**, *14*, 1363–1376.

(16) Lopata, K.; Van Kuiken, B. E.; Khalil, M.; Govind, N. Linear-Response and Real-Time Time-Dependent Density Functional Theory Studies of Core-Level Near-Edge X-Ray Absorption. *J. Chem. Theory Comput.* **2012**, *8*, 3284–3292.

(17) Fuks, J. I.; Elliott, P.; Rubio, A.; Maitra, N. T. Dynamics of Charge-Transfer Processes with Time-Dependent Density Functional Theory. *J. Phys. Chem. Lett.* **2013**, *4*, 735–739.

(18) Ding, F.; Chapman, C. T.; Liang, W.; Li, X. Mechanisms of Bridge-Mediated Electron Transfer: A TDDFT Electronic Dynamics Study. *J. Chem. Phys.* **2012**, *137*, 22A512.

(19) Rozzi, C. A.; Falke, S. M.; Spallanzani, N.; Rubio, A.; Molinari, E.; Brida, D.; Maiuri, M.; Cerullo, G.; Schramm, H.; Christoffers, J.; Lienau, C. Quantum Coherence

Controls the Charge Separation in a Prototypical Artificial Light-Harvesting System. *Nat. Commun.* **2013**, *4*, 1602.

(20) Petrone, A.; Lingerfelt, D. B.; Rega, N.; Li, X. From Charge-Transfer to a Charge-Separated State: A Perspective from the Real-Time TDDFT Excitonic Dynamics. *Phys. Chem. Chem. Phys.* **2014**, *16*, 24457–24465.

(21) Vacher, M.; Steinberg, L.; Jenkins, A. J.; Bearpark, M. J.; Robb, M. A. Electron Dynamics Following Photoionization: Decoherence due to the Nuclear-Wave-Packet Width. *Phys. Rev. A* **2015**, *92*, 040502.

(22) Jenkins, A. J.; Vacher, M.; Bearpark, M. J.; Robb, M. A. Nuclear Spatial Delocalization Silences Electron Density Oscillations in 2-Phenyl-Ethyl-Amine (PEA) and 2-Phenylethyl-N,N-Dimethylamine (PENNA) Cations. *J. Chem. Phys.* **2016**, *144*, 104110.

(23) Castro, A.; Appel, H.; Oliveira, M.; Rozzi, C. A.; Andrade, X.; Lorenzen, F.; Marques, M. A. L.; Gross, E. K. U.; Rubio, A. Octopus: A Tool for the Application of Time-dependent Density Functional Theory. *Phys. Status Solidi B* **2006**, *243*, 2465–2488.

(24) DePrince III, A. E.; Pelton, M.; Guest, J. R.; Gray, S. K. Emergence of Excited-State Plasmon Modes in Linear Hydrogen Chains from Time-Dependent Quantum Mechanical Methods. *Phys. Rev. Lett.* **2011**, *107*, 196806.

(25) Li, X.; Tully, J. C.; Schlegel, H. B.; Frisch, M. J. Ab Initio Ehrenfest Dynamics. *J. Chem. Phys.* **2005**, *123*, 084106.

(26) Liang, W.; Chapman, C. T.; Li, X. Efficient First-Principles Electronic Dynamics. *J. Chem. Phys.* **2011**, *134*, 184102.

(27) Ding, F.; Goings, J. J.; Frisch, M. J.; Li, X. Ab Initio Non-Relativistic Spin Dynamics. *J. Chem. Phys.* **2014**, *141*, 214111.

(28) Goings, J. J.; Li, X. An Atomic Orbital Based Real-Time Time-Dependent Density Functional Theory for Computing Electronic Circular Dichroism Band Spectra. *J. Chem. Phys.* **2016**, *144*, 234102.

(29) Goings, J. J.; Kasper, J. M.; Egidi, F.; Sun, S.; Li, X. Real Time Propagation of the Exact Two Component Time-Dependent Density Functional Theory. *J. Chem. Phys.* **2016**, *145*, 104107.

(30) Kasper, J. M.; Lestrange, P. J.; Stetina, T. F.; Li, X. Modeling L2,3-Edge X-ray Absorption Spectroscopy with Real-Time Exact Two-Component Relativistic Time-Dependent Density Functional Theory. *J. Chem. Theory Comput.* **2018**, *14*, 1998–2006.

(31) Lopata, K.; Govind, N. Modeling Fast Electron Dynamics with Real-Time Time-Dependent Density Functional Theory: Application to Small Molecules and Chromophores. *J. Chem. Theory Comput.* **2011**, *7*, 1344–1355.

(32) Eshuis, H.; Balint-Kurti, G. G.; Manby, F. R. Dynamics of Molecules in Strong Oscillating Electric Fields using Time-Dependent Hartree-Fock Theory. *J. Chem. Phys.* **2008**, *128*, 114113.

(33) Ruggenthaler, M.; Bauer, D. Rabi Oscillations and Few-Level Approximations in Time-Dependent Density Functional Theory. *Phys. Rev. Lett.* **2009**, *102*, 233001.

(34) Fuks, J. I.; Helbig, N.; Tokatly, I. V.; Rubio, A. Nonlinear Phenomena in Time-Dependent Density-Functional Theory: What Rabi Oscillations Can Teach Us. *Phys. Rev. B* **2011**, *84*, 075107.

(35) Raghunathan, S.; Nest, M. Critical Examination of Explicitly Time-Dependent Density

Functional Theory for Coherent Control of Dipole Switching. *J. Chem. Theory Comput.* **2011**, *7*, 2492–2497.

(36) Provorse, M. R.; Habenicht, B. F.; Isborn, C. M. Peak-Shifting in Real-Time Time-Dependent Density Functional Theory. *J. Chem. Theory Comput.* **2015**, *11*, 4791–4802.

(37) Lestrange, P. J.; Hoffmann, M. R.; Li, X. Time-Dependent Configuration Interaction using the Graphical Unitary Group Approach: Nonlinear Electric Properties. *Adv. Quantum Chem.* **2017**, *76*, 295–313.

(38) Peng, W. T.; Fales, B. S.; Levine, B. G. Simulating Electron Dynamics of Complex Molecules with Time-Dependent Complete Active Space Configuration Interaction. *J. Chem. Theory Comput.* **2018**, *14*, 4129–4138.

(39) Fales, B. S.; Levine, B. G. Nanoscale Multireference Quantum Chemistry: Full Configuration Interaction on Graphical Processing Units. *J. Chem. Theory Comput.* **2015**, *11*, 4708–4716.

(40) Shu, Y.; Hohenstein, E. G.; Levine, B. G. Configuration Interaction Singles Natural Orbitals: An Orbital Basis for an Efficient and size Intensive Multireference Description of Electronic Excited States. *J. Chem. Phys.* **2015**, *142*, 024102.

(41) Ulusoy, I. S.; Stewart, Z.; Wilson, A. K. The Role of the CI Expansion Length in Time-Dependent Studies. *J. Chem. Phys.* **2018**, *148*, 014107.

(42) Reichardt, C. Solvatochromic Dyes as Solvent Polarity Indicators. *Chem. Rev.* **1994**, *94*, 2319–2358.

(43) Stratt, R. M.; Maroncelli, M. Nonreactive Dynamics in Solution: The Emerging Molecular View of Solvation Dynamics and Vibrational Relaxation. *J. Phys. Chem.* **1996**, *100*, 12981–12996.

(44) Maroncelli, M.; Jr, E. W. C.; Bagchi, B.; Fleming, G. R. Dipolar Solvation Dynamics. *Faraday Discuss.* **1988**, *85*, 199–210.

(45) Jimenez, R.; Fleming, G. R.; Kumar, P. V.; Maroncelli, M. Femtosecond Solvation Dynamics of Water. *Nature* **1994**, *369*, 471–473.

(46) Castner Jr, E. W.; Maroncelli, M.; Fleming, G. R. Subpicosecond Resolution Studies of Solvation Dynamics in Polar Aprotic and Alcohol Solvents. *J. Chem. Phys.* **1987**, *86*, 1090–1097.

(47) Day, P. N.; Jensen, J. H.; Gordon, M. S.; Webb, S. P.; Stevens, W. J.; Krauss, M.; Garmer, D.; Basch, H.; Cohen, D. An Effective Fragment Method for Modeling Solvent Effects in Quantum Mechanical Calculations. *J. Chem. Phys.* **1998**, *105*, 1968–1986.

(48) Kairys, V.; Jensen, J. H. QM/MM Boundaries Across Covalent Bonds: A Frozen Localized Molecular Orbital-Based Approach for the Effective Fragment Potential Method. *J. Phys. Chem. A* **2000**, *104*, 6656–6665.

(49) Curutchet, C.; Muñoz-Losa, A.; Monti, S.; Kongsted, J.; Scholes, G. D.; Mennucci, B. Electronic Energy Transfer in Condensed Phase Studied by a Polarizable QM/MM Model. *J. Chem. Theory Comput.* **2009**, *5*, 1838–1848.

(50) Caprasecca, S.; Jurinovich, S.; Viani, L.; Curutchet, C.; Mennucci, B. Geometry Optimization in Polarizable QM/MM Models: The Induced Dipole Formulation. *J. Chem. Theory Comput.* **2014**, *10*, 1588–1598.

(51) Caprasecca, S.; Jurinovich, S.; Lagardère, L.; Stamm, B.; Lipparini, F. Achieving Linear Scaling in Computational Cost for a Fully Polarizable MM/Continuum Embedding. *J. Chem. Theory Comput.* **2015**, *11*, 694–704.

(52) Mao, Y.; Demerdash, O.; Head-Gordon, M.; Head-Gordon, T. Assessing Ion–Water

Interactions in the AMOEBA Force Field Using Energy Decomposition Analysis of Electronic Structure Calculations. *J. Chem. Theory Comput.* **2016**, *12*, 5422–5437.

(53) Loco, D.; Polack, É.; Caprasecca, S.; Lagardère, L.; Lipparini, F.; Piquemal, J.-P.; Mennucci, B. A QM/MM Approach Using the AMOEBA Polarizable Embedding: From Ground State Energies to Electronic Excitations. *J. Chem. Theory Comput.* **2016**, *12*, 3654–3661.

(54) Rick, S. W.; Berne, B. J. Dynamical Fluctuating Charge Force Fields: The Aqueous Solvation of Amides. *J. Am. Chem. Soc.* **1996**, *118*, 672–679.

(55) Rick, S. W.; Stuart, S. J.; Berne, B. J. Dynamical Fluctuating Charge Force Fields: Application to Liquid Water. *J. Chem. Phys.* **1998**, *101*, 6141–6156.

(56) Lipparini, F.; Barone, V. Polarizable Force Fields and Polarizable Continuum Model: A Fluctuating Charges/PCM Approach. 1. Theory and Implementation. *J. Chem. Theory Comput.* **2011**, *7*, 3711–3724.

(57) Lipparini, F.; Cappelli, C.; Barone, V. Linear Response Theory and Electronic Transition Energies for a Fully Polarizable QM/Classical Hamiltonian. *J. Chem. Theory Comput.* **2012**, *8*, 4153–4165.

(58) Boulanger, E.; Thiel, W. Solvent Boundary Potentials for Hybrid QM/MM Computations Using Classical Drude Oscillators: A Fully Polarizable Model. *J. Chem. Theory Comput.* **2012**, *8*, 4527–4538.

(59) Hedegård, E. D.; List, N. H.; Jensen, H. J. A.; Kongsted, J. The Multi-Configuration Self-Consistent Field Method Within a Polarizable Embedded Framework. *J. Chem. Phys.* **2013**, *139*, 044101.

(60) Roos, B. O.; Taylor, P. R.; Siegbahn, P. E. M. A Complete Active Space SCF Method

(CASSCF) Using a Density Matrix Formulated Super-CI Approach. *Chem. Phys.* **1980**, *48*, 157–173.

(61) Jensen, H. J. A.; Ågren, H. A Direct, Restricted-step, Second-order MC SCF Program for Large Scale ab initio Calculations. *Chem. Phys.* **1986**, *104*, 229–250.

(62) Li, Q.; Mennucci, B.; Robb, M. A.; Blancafort, L.; Curutchet, C. Polarizable QM/MM Multiconfiguration Self-Consistent Field Approach with State-Specific Corrections: Environment Effects on Cytosine Absorption Spectrum. *J. Chem. Theory Comput.* **2015**, *11*, 1674–1682.

(63) Donati, G.; Wildman, A.; Caprasecca, S.; Lingerfelt, D. B.; Lipparini, F.; Mennucci, B.; Li, X. Coupling Real-Time Time-Dependent Density Functional Theory with Polarizable Force Field. *J. Phys. Chem. Lett.* **2017**, *8*, 5283–5289.

(64) Werner, H. J.; Meyer, W. A Quadratically Convergent MCSCF Method for the Simultaneous Optimization of Several States. *J. Chem. Phys.* **1981**, *74*, 5794–5801.

(65) Leforestier, C.; Bisseling, R. H.; Cerjan, C.; Feit, M. D.; Friesner, R.; Guldberg, A.; Hammerich, A.; Jolicard, G.; Karrlein, W.; Meyer, H.-D.; Lipkin, N.; Roncero, O.; Kosloff, R. A Comparison of Different Propagation Schemes for the Time Dependent Schrödinger Equation. *J. Chem. Phys.* **1991**, *94*, 59–80.

(66) Gray, S. K.; Noid, D. W.; Sumpter, B. Symplectic Integrators for Large Scale Molecular Dynamics Simulations: A Comparison of Several Explicit Methods. *J. Chem. Phys.* **1994**, *101*, 4062–4072.

(67) Blanes, S.; Casas, F.; Murua, A. Symplectic Splitting Operator Methods for the Time-dependent Schrödinger Equation. *J. Chem. Phys.* **2006**, *124*, 234105.

(68) Olsen, J.; Roos, B. O.; Jørgensen, P. Determinant Based Configuration Interaction

Algorithms for Complete and Restricted Configuration Interaction Spaces. *J. Chem. Phys.* **1988**, *89*, 2185–2192.

(69) Thole, B. T. Molecular Polarizabilities Calculated with a Modified Dipole Interaction. *Chem. Phys.* **1981**, *59*, 341–350.

(70) van Duijnen, P. T.; Swart, M. Molecular and Atomic Polarizabilities: Thole's Model Revisited. *J. Phys. Chem. A* **1998**, *102*, 2399–2407.

(71) Wang, J.; Cieplak, P.; Li, J.; Hou, T.; Luo, R.; Duan, Y. Development of Polarizable Models for Molecular Mechanical Calculations I: Parameterization of Atomic Polarizability. *J. Phys. Chem. B* **2011**, *115*, 3091–3099.

(72) Caprasecca, S.; Curutchet, C.; Jurinovich, S.; Mennucci, B. PolChat: A Polarisation-Consistent Charge Fitting Tool, Molecolab Tools. 2017.

(73) Jurinovich, S.; Curutchet, C.; Mennucci, B. The Fenna–Matthews–Olson Protein Revisited: A Fully Polarizable (TD)DFT/MM Description. *ChemPhysChem* **2014**, *15*, 3194–3204.

(74) Wildman, A.; Donati, G.; Lipparini, F.; Mennucci, B.; Li, X. Nonequilibrium Environment Dynamics in a Frequency-Dependent Polarizable Embedding Model. *J. Chem. Theory Comput.* **2019**, *15*, 43–51.

(75) Bruner, A.; LaMaster, D.; Lopata, K. Accelerated Broadband Spectra Using Transition Dipole Decomposition and Padé Approximants. *J. Chem. Theory Comput.* **2016**, *12*, 3741–3750.

(76) Frisch, M. J.; Trucks, G. W.; Schlegel, H. B.; Scuseria, G. E.; Robb, M. A.; Cheeseman, J. R.; Scalmani, G.; Barone, V.; Petersson, G. A.; Nakatsuji, H.; Li, X.; Caricato, M.; Marenich, A. V.; Bloino, J.; Janesko, B. G.; Gomperts, R.; Mennucci, B.; Hratchian, H. P.; Ortiz, J. V.; Izmaylov, A. F.; Sonnenberg, J. L.; Williams-

Young, D.; Ding, F.; Lipparini, F.; Egidi, F.; Goings, J.; Peng, B.; Petrone, A.; Henderson, T.; Ranasinghe, D.; Zakrzewski, V. G.; Gao, J.; Rega, N.; Zheng, G.; Liang, W.; Hada, M.; Ehara, M.; Toyota, K.; Fukuda, R.; Hasegawa, J.; Ishida, M.; Nakajima, T.; Honda, Y.; Kitao, O.; Nakai, H.; Vreven, T.; Throssell, K.; Montgomery, J. A., Jr.; Peralta, J. E.; Ogliaro, F.; Bearpark, M. J.; Heyd, J. J.; Brothers, E. N.; Kudin, K. N.; Staroverov, V. N.; Keith, T. A.; Kobayashi, R.; Normand, J.; Raghavachari, K.; Rendell, A. P.; Burant, J. C.; Iyengar, S. S.; Tomasi, J.; Cossi, M.; Millam, J. M.; Klene, M.; Adamo, C.; Cammi, R.; Ochterski, J. W.; Martin, R. L.; Morokuma, K.; Farkas, O.; Foresman, J. B.; Fox, D. J. Gaussian Development Version Revision I.10+.

(77) Maroncelli, M.; Fleming, G. R. Picosecond Solvation Dynamics of Coumarin 153: The Importance of Molecular Aspects of Solvation. *J. Chem. Phys.* **1987**, *86*, 6221–6239.

(78) Lewis, J. E.; Maroncelli, M. On the (Uninteresting) Dependence of the Absorption and Emission Transition Moments of Coumarin 153 on Solvent. *Chem. Phys. Lett.* **1998**, *282*, 197–203.

(79) Kovalenko, S. A.; Ruthmann, J.; Ernsting, N. P. Ultrafast Stokes Shift and Excited-State Transient Absorption of Coumarin 153 in Solution. *Chem. Phys. Lett.* **1997**, *271*, 40–50.

(80) Horng, M. L.; Gardecki, J. A.; Papazyan, A.; Maroncelli, M. Subpicosecond Measurements of Polar Solvation Dynamics: Coumarin 153 Revisited. *J. Phys. Chem.* **1995**, *99*, 17311–17337.

(81) Kumar, P. V.; Maroncelli, M. Polar Solvation Dynamics of Polyatomic Solutes: Simulation Studies in Acetonitrile and Methanol. *J. Chem. Phys.* **1995**, *103*, 3038–3059.

(82) Reynolds, L.; Gardecki, J. A.; Frankland, S. J. V.; Horng, M. L.; Maroncelli, M. Dipole Solvation in Nondipolar Solvents: Experimental Studies of Reorganization Energies and Solvation Dynamics. *J. Phys. Chem.* **1996**, *100*, 10337–10354.

(83) Cave, R. J.; E. W. Castner, J. Time-Dependent Density Functional Theory Investigation of the Ground and Excited States of Coumarins 102, 152, 153, and 343. *J. Phys. Chem. A* **2002**, *106*, 12117–12123.

(84) Improta, R.; Barone, V.; Scalmani, G.; Frisch, M. J. A State-Specific Polarizable Continuum Model Time Dependent Density Functional Theory Method for Excited State Calculations in Solution. *J. Chem. Phys.* **2006**, *125*, 054103.

(85) Mühlpfordt, A.; Schanz, R.; Ernsting, N. P.; Farztdinov, V.; Grimme, S. Coumarin 153 in the Gas Phase: Optical Spectra and Quantum Chemical Calculations. *Phys. Chem. Chem. Phys.* **1999**, *1*, 3209–3218.

(86) Kurashige, Y.; Nakajima, T.; Kurashige, S.; Hirao, K.; Nishikitani, Y. Theoretical Investigation of the Excited States of Coumarin Dyes for Dye-Sensitized Solar Cells. *J. Phys. Chem. A* **2007**, *111*, 5544–5548.

(87) O'Regan, B.; Grätzel, M. A Low-Cost, High-Efficiency Solar Cell Based on Dye-Sensitized Colloidal TiO_2 Films. *Nature* **1991**, *353*, 737–740.

(88) Adamo, C.; Barone, V. Toward Reliable Density Functional Methods without Adjustable Parameters: The PBE0 Model. *J. Chem. Phys.* **1999**, *110*, 6158–6170.

(89) Ditchfield, R.; Hehre, W. J.; Pople, J. A. Self-Consistent Molecular-Orbital Methods. IX. An Extended Gaussian-Type Basis for Molecular-Orbital Studies of Organic Molecules. *J. Chem. Phys.* **1971**, *54*, 724–728.

(90) Francl, M. M.; Pietro, W. J.; Hehre, W. J.; Binkley, J. S.; Gordon, M. S.; DeFrees, D. J.; Pople, J. A. Self-Consistent Molecular Orbital Methods. XXIII. A Polarization Type Basis Set for Second Row Elements. *J. Chem. Phys.* **1982**, *77*, 3654–3665.

(91) Wang, J.-P.; Chen, J.-S.; Zhao, G.-J. Steady-State and Time-Resolved Spectroscopic

Investigations on the Existence of Stable Methanol/AOT/n-Heptane Reverse Micelles. *J. Colloid Interface Sci.* **2014**, *423*, 1–6.

(92) Królicki, R.; Jarzęba, W.; Mostafavi, M.; Lampre, I. Preferential Solvation of Coumarin 153 - The Role of Hydrogen Bonding. *J. Phys. Chem. A* **2002**, *106*, 1708–1713.

(93) Jacquemin, D.; Planchat, A.; Adamo, C.; Mennucci, B. TD-DFT Assessment of Functionals for Optical 0-0 Transitions in Solvated Dyes. *J. Chem. Theory Comput.* **2012**, *8*, 2359–2372.

(94) Improta, R.; Barone, V.; Santoro, F. Ab Initio Calculations of Absorption Spectra of Large Molecules in Solution: Coumarin 153. *Angew. Chem.* **2007**, *119*, 409–412.

(95) Cornell, W. D.; Cieplak, P.; Bayly, C. I.; Gould, I. R.; Merz, K. M.; Ferguson, D. M.; Spellmeyer, D. C.; Fox, T.; Caldwell, J. W.; Kollman, P. A. A Second Generation Force Field for the Simulation of Proteins, Nucleic Acids, and Organic Molecules. *J. Am. Chem. Soc.* **1995**, *117*, 5179–5197.

(96) Wang, J.; Cieplak, P.; Kollman, P. A. How Well Does a Restrained Electrostatic Potential (RESP) Model Perform in Calculating Conformational Energies of Organic and Biological Molecules? *J. Comput. Chem.* **2000**, *21*, 1049–1074.

(97) Hornak, V.; Abel, R.; Okur, A.; Strockbine, B.; Roitberg, A.; Simmerling, C. Comparison of Multiple Amber Force Fields and Development of Improved Protein Backbone Parameters. *Proteins* **2006**, *65*, 712–725.

Graphical TOC Entry